^{113}Cd β-decay spectrum and g_A quenching using spectral moments

Joel Kostensalo,[1] Eligio Lisi,[2] Antonio Marrone,[3,2] and Jouni Suhonen[4]
[1]*Natural Resources Institute Finland, Yliopistokatu 6B, FI-80100 Joensuu, Finland*
[2]*Istituto Nazionale di Fisica Nucleare, Sezione di Bari, Via Orabona 4, 70126 Bari, Italy*
[3]*Dipartimento Interateneo di Fisica "Michelangelo Merlin," Via Amendola 173, 70126 Bari, Italy*
[4]*Department of Physics, University of Jyväskylä, P.O. Box 35, FI-40014, Jyväskylä, Finland*

(Received 15 February 2023; revised 24 March 2023; accepted 9 May 2023; published 18 May 2023)

We present an alternative analysis of the ^{113}Cd β-decay electron energy spectrum in terms of spectral moments μ_n, corresponding to the averaged values of nth powers of the β particle energy. The zeroth moment μ_0 is related to the decay rate, while higher moments μ_n are related to the spectrum shape. The here advocated spectral-moment method (SMM) allows for a complementary understanding of previous results, obtained using the so-called spectrum-shape method (SSM) and its revised version, in terms of two free parameters: $r = g_A/g_V$ (the ratio of axial-vector to vector couplings) and s (the small vectorlike relativistic nuclear matrix element, s-NME). We present numerical results for three different nuclear models with the conserved vector current hypothesis (CVC) assumption of $g_V = 1$. We show that most of the spectral information can be captured by the first few moments, which are simple quadratic forms (conic sections) in the (r, s) plane: An ellipse for $n = 0$ and hyperbolas for $n \geqslant 1$, all being nearly degenerate as a result of cancellations among nuclear matrix elements. The intersections of these curves, as obtained by equating theoretical and experimental values of μ_n, identify the favored values of (r, s) at a glance, without performing detailed fits. In particular, we find that values around $r \approx 1$ and $s \approx 1.6$ are consistently favored in each nuclear model, confirming the evidence for g_A quenching in ^{113}Cd, and shedding light on the role of the s-NME. We briefly discuss future applications of the SMM to other forbidden β-decay spectra sensitive to g_A.

DOI: 10.1103/PhysRevC.107.055502

I. INTRODUCTION

The search for the rare process of neutrinoless double beta decay ($0\nu\beta\beta$), as well the study of its implications for the fundamental nature of the neutrino field (Dirac or Majorana), represent a major topic in both particle and nuclear physics [1–3]. The predicted rate of this decay, as well as of other weak-interaction nuclear processes, depends sensitively on the effective value of the weak axial-vector coupling g_A that, in nuclear matter, appears to be generally different [4,5] from the vacuum value $g_A^{vac} = 1.276$ [6,7]. In particular, effective quenching factors $q = g_A/g_A^{vac} < 1$ have been discussed in a variety of observed β and $\beta\beta$ decays, whose Gamow-Teller (GT) nuclear matrix elements are reduced by factors of q and q^2, respectively; see, e.g., [4,5,8–11].

While the theoretical connections among disparate values of q and their physical origin are still subject to research [4,12–14], from a phenomenological viewpoint it makes sense to study observables that appear to be particularly sensitive to possible quenching effects. In this context, highly forbidden nonunique β decays offer a very interesting avenue, since both their calculated decay rates and energy-spectrum shapes are found to change very rapidly around quenched values $g_A \approx 1$, due to subtle cancellations among large nuclear matrix elements (NME) [15].

For the fourth-forbidden nonunique β decay of ^{113}Cd, detailed experimental data are available for the energy spectrum $S(w_e)$ in terms of the β energy w_e [16,17]. The data constrain both the overall decay rate (or, analogously, the half-life) and the energy spectrum shape (as a function of w_e). It is highly nontrivial to match the corresponding theoretical predictions with data, since the values of g_A that best fit the decay half-life are not necessarily the same that best fit the decay spectral shape and may be in conflict [15,17,18], although both indicate large NME cancellations. These two approaches to constraining g_A in ^{113}Cd β decay, dubbed as half-life and spectrum-shape methods [18], have only recently been reconciled by varying a small parameter multiplied by the vector coupling g_V, namely, the so-called small relativistic nuclear matrix element s-NME [19] ($^{V}\mathcal{M}^{(0)}_{431}$ in the notation of Behrens and Bühring [20]), the estimates of which, from the conserved vector current (CVC) hypothesis or based on specific nuclear models, are rather uncertain but crucial for forbidden decays [21,22].

In particular, by treating the s-NME as a free parameter to be determined by data in a revised version of the spectrum-shape method (SSM) [19], both the ^{113}Cd half-life and spectrum data in [19,23] have been found to match well the theoretical predictions of different models, with consistent values of the quenching factor and the s-NME. These nontrivial results, which represent a strong indication for g_A quenching in ^{113}Cd, deserve in our opinion further analysis, aiming at a better understanding of the comparison of theory and data, in light of recent and future investigations of forbidden

β-decay spectra in other nuclides [22,24,25]. In particular, we aim at reducing the relevant spectral information to a relatively small set of quantities or parameters to be studied.

We start from the basic property that any smooth spectrum $S(w_e)$ can be characterized by (and reconstructed from) the series of its moments μ_n, namely, by the spectrum-averaged values of w_e^n for $n \geqslant 0$ [26,27]. This approach to spectra allows for the unification of the half-life method (connected to μ_0) and the SSM (connected to $\mu_{1,2,3,\ldots}$) in a single "spectral-moment method" (SMM). We show that a few moments μ_n can capture with high accuracy the whole spectral information in terms of the two free parameters, $r = g_A/g_V$ and $s = s$-NME, where g_V is the vector coupling (assumed to be unity as in [19]). Furthermore, since the moments μ_n are simple quadratic forms in (r, s), the information contained in the infinite family of spectra $S(w_e \,|\, r, s)$ can be eventually discretized, with significant conceptual and numerical advantages.

Concerning experimental data, herein we use the absolute ^{113}Cd β-decay spectrum of [16] including the energy calibration and systematics assessment performed in [28]. Constraints on (r, s), as obtained by comparing theoretical and experimental moments, are interpreted in terms of intersections of isomoment curves (an ellipse for μ_0 and hyperbolas for $\mu_{1,2,3,\ldots}$). In each of three different nuclear models for the NME, such intersections are closest for rather similar values of the (r, s) parameters. Since most of the relevant features appear to be captured by just the first few moments, the method can be pragmatically applied to future forbidden β-decay measurements in different nuclei, where the available spectral data might be more limited than for ^{113}Cd.

Our work is structured as follows. In Sec. II we discuss the spectral-moment method, the adopted notation, and the numerical values of the first few moments. In Sec. III we discuss the implications of equating the theoretical and experimental moments in terms of the (r, s) parameters. We find evidence for $r \approx 1$, corresponding to a multiplicative renormalization of the axial-vector coupling, as well as for $|s| \approx 1.6$ (with a preference for positive values of s), corresponding to an additive contribution to vectorlike NME, consistent with earlier findings utilizing a different approach and independent data [19]. We summarize our results and consider further applications of the SMM in Sec. IV. Technical aspects about NMEs and quadratic forms are discussed in Appendices A and B, respectively.

II. SPECTRAL MOMENTS: METHOD, NOTATION, AND NUMERICAL VALUES

In this section we define the notation used in the SMM to describe the ^{113}Cd β-decay spectra (experimental and theoretical) in terms of a truncated set of spectral moments. Numerical values for such moments are also derived.

A. β-decay spectrum notation

Following [15,18,19], we introduce a dimensionless energy parameter w_e,

$$w_e = \frac{W_e}{m_e} = 1 + \frac{T_e}{m_e}, \tag{1}$$

where W_e and T_e are, respectively, the total and kinetic energies of the electron with mass m_e.

The energy spectrum $S(w_e)$ is defined as the fractional number of decays n_e per single nucleus and per unit of time t and of energy w_e:

$$S(w_e) = \frac{d^2 n_e}{dt\, dw_e}, \tag{2}$$

where $w_e \in [1,\ w_0]$, and the endpoint w_0 is set by the Q_β value of the decay ($w_0 = 1 + Q_\beta/m_e$). When needed, experimental (e) and theoretical (t) spectra are distinguished by superscripts,

$$S^e = S^{\text{expt}}, \tag{3}$$

$$S^t = S^{\text{theo}}. \tag{4}$$

In order to link our formalism with common nuclear physics notation, we remind that the total decay rate λ (or, equivalently, the half-life $t_{1/2}$) is obtained by integrating $S(w_e)$ over the interval $[1,\ w_0]$:

$$\lambda = \int_1^{w_0} S(w_e)\, dw_e = \frac{\ln 2}{t_{1/2}}. \tag{5}$$

However, we shall not use either λ or $t_{1/2}$ hereafter, for the following reason.

Due to increasingly high backgrounds at low energy, the experimental spectrum is typically reported above a detector-dependent kinetic energy threshold $T_{\text{thr}} > 0$ [16,17,19,28] that defines the w_e threshold as $w_{\text{thr}} = 1 + T_{\text{thr}}/m_e > 1$. Therefore, the decay half-life $t_{1/2}$ can be estimated only by extrapolating the measured S^e spectrum down to $T \to 0$; see, e.g., [16]. However, any adopted extrapolation function may well be different from the computed theoretical spectra in the range $[1,\ w_{\text{thr}}]$ below threshold. In order to avoid potential biases, we shall thus consistently compare the experimental and theoretical spectra only in the energy range above threshold,

$$w_e \in [w_{\text{thr}},\ w_0]. \tag{6}$$

B. Spectral moments μ_n

It is well known from statistics that a smooth spectrum $S(w_e)$, defined over an interval $w_e \in [w_{\text{thr}},\ w_0]$, can be described by a series of moments $\{\mu_n\}_{n\geqslant 0}$ [26,29]. The zeroth moment, defined as

$$\mu_0 = \int_{w_{\text{thr}}}^{w_0} S(w_e)\, dw_e, \tag{7}$$

encodes the overall spectrum normalization, while the first and higher moments, defined as

$$\mu_n = \frac{\int_{w_{\text{thr}}}^{w_0} S(w_e)\, w_e^n\, dw_e}{\int_{w_{\text{thr}}}^{w_0} S(w_e)\, dw_e} \quad (n \geqslant 1), \tag{8}$$

encode the spectrum shape information, via the averaged values of increasingly high powers of the main variable.[1]

[1]The so-called central moments, not used herein, are alternatively defined by averaging the powers $(w_e - \mu_1)^n$ for $n \geqslant 2$. The second

Note that, in our case, μ_0 has the dimension of an inverse time, being defined as the decay rate in the interval $[w_{\rm thr},\ w_0]$ above threshold (see also Eq. (5) for the total rate in $[1,\ w_0]$). All the other moments are instead dimensionless. When needed, moments of theoretical and experimental spectra will be distinguished by superscripts:

$$S = S^t \rightarrow \mu_n = \mu_n^t, \tag{9}$$

$$S = S^e \rightarrow \mu_n = \mu_n^e. \tag{10}$$

There is vast, interdisciplinary literature on the inverse moment problem, namely, on possible methods to reconstruct the original function $S(w_e)$ from a finite number of moments $\{\mu_n\}_{n=0,\ldots,N}$ with some approximations [27,30,31]. While all methods tend to improve their accuracy for increasing N, some may converge faster or better than others, depending on specific features of the function(s) $S(w_e)$.

We have checked that a simple reconstruction algorithm based on an expansion in Legendre polynomials, as described in [32], is sufficient enough to allow for the reconstruction of the ^{113}Cd spectra at subpercent level (more accurately than is needed for our purposes) in the entire parameter space relevant for this work, with just $N = 6$ moments. Representative examples of theoretical spectra reconstructed from a finite set of moments are shown below in Sec. II D. Such results are consistent with (but more general than) the findings of Ref. [16], where the experimental spectrum was well approximated in terms of a sixth-order polynomial function.

We shall thus limit ourselves to $N = 6$ and consider the truncated set of moments

$$\{\mu_n\} = \mu_0,\ \mu_1, \ldots,\ \mu_6. \tag{11}$$

Actually, as we shall see in several ways, interesting results can be obtained by considering just the first two or three moments out of the above set.

C. Experimental spectrum $S^e(w_e)$

In this work we consider the experimental spectrum $S_e(w_e)$ of ^{113}Cd as measured in [16], after a recalibration of the energy scale and the deconvolution of resolution effects as described in [28] (see Fig. 29 therein). The experimental threshold $T_{\rm thr} = 26$ keV [28] and the endpoint $Q_\beta = 323.83$ keV [33] define the analysis range:

$$w_e \in [w_{\rm thr},\ w_0] = [1.051,\ 1.634]. \tag{12}$$

In this range, the experiment observed $N_e = 2.222 \times 10^6$ events for $N_d = 8.858 \times 10^{22}$ decaying nuclei over a data-taking time $t = 9.929 \times 10^6$ s [16,28]. The corresponding decay rate provides the zeroth moment $\mu_0^e = N_e/(N_d\, t)$:

$$\mu_0^e = 2.526 \times 10^{-24}\ {\rm s}^{-1}. \tag{13}$$

Figure 1 shows the experimental spectrum in the range of Eq. (12), as taken from [28] with the above normalization. The spectrum is reported in bins of width $\Delta w_e = 2\ {\rm keV}/m_e$,

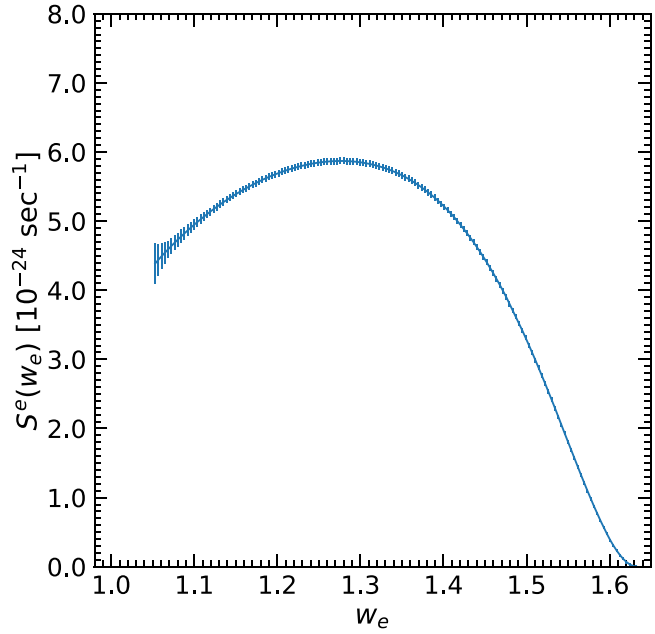

FIG. 1. Experimental energy spectrum for ^{113}Cd β decay (central values and total 1σ errors) as taken from [28]. See the text for details.

together with total (statistical and systematic) uncertainty in each bin.

From the above $S^e(w_e)$ we derive the following values for the experimental moments (up to $N = 6$):

$$\mu_1^e = 1.291, \tag{14}$$

$$\mu_2^e = 1.686, \tag{15}$$

$$\mu_3^e = 2.226, \tag{16}$$

$$\mu_4^e = 2.970, \tag{17}$$

$$\mu_5^e = 4.004, \tag{18}$$

$$\mu_6^e = 5.452. \tag{19}$$

We postpone the discussion of related uncertainties to Sec. III.

A final comment is in order. In [16], by extrapolating the observed spectrum below threshold (i.e., for $w_e \in [1,\ 1.051]$), the total number of decays was estimated to be $N_e' = 2.40 \times 10^6$ for the exposure $N_d\, t$, corresponding to a decay rate $\lambda = N_e'/(N_d\, t) = 2.73 \times 10^{-24}$ s^{-1} and to the quoted half-life $t_{1/2} = \ln 2/\lambda = 8.04 \times 10^{15}$ yr. As previously mentioned, we do not use extrapolated quantities such as λ or $t_{1/2}$ in this work.

D. Theoretical spectrum $S^t(w_e)$ and its free parameters $(r,\ s)$

As discussed in [18] and references therein, the theoretical β-decay spectrum $S^t(w_e)$ can be generally expressed as

$$S^t(w_e) = \frac{\ln 2}{\kappa}\, C(w_e)\, p\, w_e\, (w_0 - w_e)^2\, F_0(Z,\ w_e), \tag{20}$$

central moment is the variance, the third the skewness, and the fourth the kurtosis.

where $C(w_e)$ is the so-called shape factor, p is the electron momentum in units of m_e, and $F_0(Z,\ w_e)$ is the Fermi function with the final nuclear state having $Z = 49$. In contexts where extreme precision is required, small correction terms accounting for, e.g., radiative effects and atomic screening become important. For the purposes of this work these $\approx$1% corrections are insignificant but have been included as described in [18]. The conversion constant κ reads

$$\kappa = \frac{2\pi^3 \ln 2}{m_e^5\,(G_F\ \cos\theta_C)^2} = 6289\ \text{s}, \tag{21}$$

where G_F is the Fermi constant and θ_C is the Cabibbo angle. For nonunique decays the shape factor has a complicated expression including universal kinematic factors and nuclear matrix elements (NME). The latter capture all the nuclear-structure dependent information regarding the decay. In the formalism of Behrens and Bühring [20] the NME arise from a multipole expansion of the nuclear current. The NME are then expanded as a power series resulting in an expression including vector NME ${}^V\mathcal{M}^{(m)}_{KLs}$ and axial-vector NME ${}^A\mathcal{M}^{(m)}_{KLs}$. The matrix elements with the smallest angular momenta K and L allowing for the decay dominate, with the first term in the power series, $m = 0$, being by far the most important. For fourth-forbidden unique decays there are four leading-order NME, with the dominant matrix elements being ${}^V\mathcal{M}^{(0)}_{440}$ and ${}^A\mathcal{M}^{(0)}_{441}$, and with significantly smaller contributions coming from ${}^V\mathcal{M}^{(0)}_{431}$ and ${}^A\mathcal{M}^{(0)}_{541}$. The expansion can be further carried out to next-to-leading order, resulting in a total of 45 NME [18] that depend on w_e and on powers of the nuclear radius $R = 1.2A^{1/3}$ fm $= 5.8$ fm. The NME need to be numerically computed with specific nuclear models. Following [18,19] we consider the microscopic interacting boson-fermion model (IBFM-2), the microscopic quasiparticle-phonon model (MQPM), and the interacting shell model (ISM). First we discuss general aspects of the spectrum structure, and then report model-dependent numerical results in terms of spectral moments.

In general, $C(w_e)$ is a sum over squares and products of linear combinations of NME, each being multiplied by either the vector coupling $g_{\rm V}$ or the axial-vector coupling $g_{\rm A}$. The couplings arise in the formalism of beta decays as a means to normalize the hadron current when moving from the quark level to the level of nucleons, and each axial-vector matrix element is always preceded by $g_{\rm A}$ and each vector matrix element by $g_{\rm V}$. By defining the ratio

$$r = g_{\rm A}/g_{\rm V} \tag{22}$$

one can formally write $S^t(w_e)$ as a quadratic form in r [15],

$$S^t = g_{\rm V}^2\left(S^t_{\rm V} + rS^t_{\rm VA} + r^2S^t_{\rm A}\right), \tag{23}$$

where $S^t_{\rm A}$ includes only axial-vector NME, $S^t_{\rm V}$ only vector NME, and $S^t_{\rm VA}$ is a mix of vector and axial-vector NME. Hereafter we shall assume as in [19], in accordance with the conserved vector current (CVC), that

$$g_{\rm V} = 1, \tag{24}$$

while r will be treated as a free theoretical parameter to be fixed by the data. We shall comment on deviations from Eq. (24) in Sec. III.

As discussed in detail in [18], the quadratic form in Eq. (23) entails delicate cancellations among large NME for $r \approx 1$, where agreement between theory and data can be usually found in terms of either the spectrum normalization [15] or its shape [17], but not both at the same time (as far as r is the only free parameter) [15,18]. In particular, the main NME cancellation term turns out to be the square of a binomial, up to subleading NME terms ϵ and ϵ':

$$S^t \propto \left({}^V\mathcal{M}^{(0)}_{440} - \alpha\ {}^A\mathcal{M}^{(0)}_{441}\, r + \epsilon\right)^2 + \epsilon', \tag{25}$$

where α is a numerical coefficient of $O(1)$ and the $\mathcal{M}$'s are "large" NME, typically of $O(10^2)$–$O(10^3)$ in units of fm^4; see [18] for details of the notation and for numerical $\mathcal{M}$ values in the various nuclear models. For $r \approx 1$, it turns out that the two large $\mathcal{M}$'s tend to cancel each other, leaving a residual of $O(1)$ [18]. Therefore, a subleading term $\epsilon \sim O(1)$ may still play a significant role, especially if its numerical value is rather uncertain.

It was realized in [19,21,22] that this role can be played by so-called small relativistic NME, dubbed the s-NME in [19] and here just as s for simplicity, where

$$s = {}^V\mathcal{M}^{(0)}_{431}, \tag{26}$$

in units of fm^3. On the one hand, with very simple (though unrealistic) assumptions related to the nuclear-structure aspects of the decay, the CVC hypothesis would imply (in our adopted units) the numerical relation ${}^V\mathcal{M}^{(0)}_{431} = 0.0678(R^{-1})\,{}^V\mathcal{M}^{(0)}_{440}$ [19], leading to expected values $s \sim O(1$–$10)$. On the other hand, numerical evaluations of s either give $s = 0$ due to model-specific limitations relating to a restricted model space (in the IBFM-2 and ISM models) or to $s \simeq 0.4$ (in the MQPM model) [18]. A more detailed discussion of the uncertain estimates of $s = {}^V\mathcal{M}^{(0)}_{431}$ as compared with ${}^V\mathcal{M}^{(0)}_{440}$ and ${}^A\mathcal{M}^{(0)}_{441}$ is presented in Appendix A.

Given such uncertainties, in [19] the s-NME was simply assumed as a free parameter, presumably of $O(1)$, to be constrained by comparison with the data (together with $g_{\rm A}$). It turns out that, in this way, both the experimental spectrum shape and its normalization can be well reproduced theoretically [19]. In the same spirit, we treat $(r,\ s)$ as free parameters in our analysis.

Figure 2 shows three representative theoretical spectra $S^t(w_e)$ calculated in the IBFM-2 model (dashed lines) for three different $(r,\ s)$ values. Their accurate reconstruction through a set of moments truncated at $N = 6$ is also shown in the left panel (dotted lines). Analogously, the right panel shows the reconstruction truncated at $N = 2$: It can be seen that the main qualitative features of the spectra are already captured by using just the first three moments μ_0, μ_1, and μ_2. Similar results hold for the spectra calculated in the MQPM and ISM models (not shown). The analysis in Sec. III will confirm that, in general, a few moments are enough to derive useful indications on the $(r,\ s)$ parameters.

In particular, by using as free parameters both r and s, it appears from Fig. 2 that one can alter both the peak position

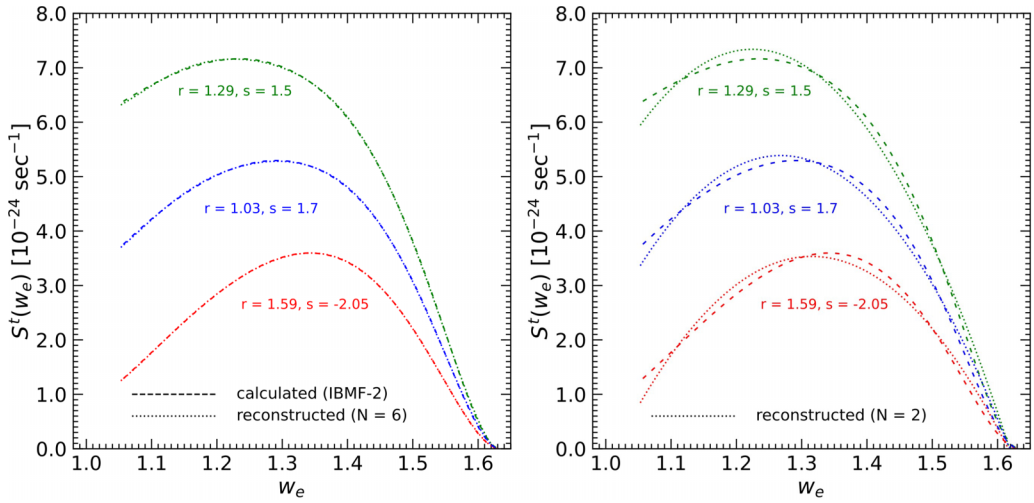

FIG. 2. Representative examples of theoretical spectra S^t as calculated in the IBFM-2 model (dashed lines), for three representative pairs of the $(r,\ s)$ parameters. The reconstruction of the spectra based on a truncated set of moments is also shown (dotted lines) for $N = 6$ (left panel) and $N = 2$ (right panel).

and the normalization of the theoretical spectrum, and may thus hope to match the experimental spectrum in Fig. 1. It turns out that this result is achieved for typical values $r \approx 1$ (confirming g_A quenching) and $s \sim O(1)$ (in the expected numerical ballpark), where the large NME cancellations mentioned in the context of Eqs. (25) and (26) take place. We shall recover very similar results, not only by using an independent data set [16,28] (as reported in Fig. 1), but by adopting a different perspective, based on the following generalization of the quadratic form in Eq. (23).

We observe that, since s adds to the NME terms multiplied by g_V, it must appear up to second power in $S^t(\omega)$. Moreover, a mixed dependence $\propto r\,s$ must emerge from the VA term in Eq. (23). Therefore, the spectrum $S^t(w_e)$ must be a quadratic form in both r and s, as well as any integral over it involving w_e^n (with $n \geqslant 0$),

$$\int_{w_{\rm thr}}^{w_0} S^t(w_e)\, w_e^n\, dw_e = \sum_{i+j\leqslant 2} a_{ij}^n\, r^i\, s^j, \tag{27}$$

where the numerical coefficients a_{ij}^n (with n being a superscript, not a power) are expressed in units of s^{-1} as the spectrum S^t. The zeroth moment $\mu_0^t(r,\ s)$ corresponds to the above quadratic form with $n = 0$, while the nth moment $\mu_n^t(r,\ s)$ for $n \geqslant 1$ corresponds to a ratio of quadratic forms (with index n at numerator and zero at denominator).

In practice, to evaluate the a_{ij}^n coefficients for a given nuclear model at fixed n, one just needs to calculate the energy spectrum $S^t(w_e \mid r,\ s)$ at six arbitrary points $(r,\ s)$, evaluate the integral on the left-hand side (l.h.s.) of Eq. (27), and solve in the six unknowns $\{a_{ij}^n\}$.[2] Table I reports the numerical $\{a_{ij}^n\}$ values (in units of 10^{-24} s^{-1}) up to $N = 6$, for the three nuclear models discussed in this work.

[2]To be sure, we have numerically checked the validity of Eq. (27) over a dense grid sampling the relevant $(r,\ s)$ parameter space, in all of the three nuclear models (IBFM-2, MQPM, and ISM).

Summarizing, we have discretized the continuous information contained in the infinite family of spectra $S^t(w_e \mid r,\ s)$ into a small number of moments μ_n^t, each depending on simple quadratic forms in the free parameters r and s (involving six coefficients a_{ij}^n at any n). This approach greatly simplifies the numerical calculation of the theoretical moments, as well as their comparison with the experimental moments μ_n^e, as discussed below.

III. SPECTRAL MOMENT METHOD: COMPARISON OF THEORY AND DATA

In this section we explore the implications of equating a finite set of theoretical and experimental moments:

$$\mu_n^t(r,\ s) = \mu_n^e\ (n = 0,\ 1, \ldots, N). \tag{28}$$

Each of the above equations sets a quadratic form in $(r,\ s)$ equal to a constant, and thus leads to a conic section in the corresponding coordinates. It turns out that, for $n = 0$, the conic section is a slanted and elongated ellipse, while for $n \geqslant 1$ the conics form a bundle of hyperbolas. In the ideal case (perfect match between theory and data), all these curves would intersect in a single $(r,\ s)$ point; in real cases, the various crossing points will cluster with some dispersion around a preferred $(r,\ s)$ region. The smaller the dispersion, the better the agreement between the experimental and theoretical moments and spectra. In Appendix B we discuss general features of the conic sections and of their crossings, that allow one to visualize the effects of large NME cancellations, as well as to interpret previous fit results obtained in [19] through the revised spectrum shape method. Below we show our results in the $(r,\ s)$ plane and discuss the preferred parameter values in the three nuclear models considered.

Figure 3 shows the loci of points in the $(r,\ s)$ plane fulfilling Eq. (28) up to $N = 6$, for the models IBMF-2 (left), MQPM (middle), and ISM (right). In each panel, one can see (part of) the slanted ellipse determined by the zeroth moment, and the bundle of hyperbolas determined by the

TABLE I. Coefficients a^n_{ij} of the quadratic forms parametrizing the theoretical moments up to $N = 6$, in each of the three nuclear models considered in this work. The a^n_{ij} are expressed in units of 10^{-24} s^{-1}.

Model	n	a^n_{20}	a^n_{02}	a^n_{11}	a^n_{10}	a^n_{01}	a^n_{00}
	0	+2.8998	+0.7914	+2.8163	−5.8662	−2.9952	+3.1087
	1	+3.6046	+1.0225	+3.5722	−7.2731	−3.7984	+3.8552
	2	+4.5331	+1.3358	+4.5835	−9.1214	−4.8722	+4.8357
IBFM-2	3	+5.7690	+1.7640	+5.9492	−11.574	−6.3214	+6.1368
	4	+7.4305	+2.3542	+7.8102	−14.862	−8.2949	+7.8803
	5	+9.6855	+3.1738	+10.368	−19.312	−11.005	+10.239
	6	+12.774	+4.3204	+13.912	−25.390	−14.758	+13.460
	0	+20.086	+0.7914	+7.5565	−41.059	−7.8113	+21.146
	1	+24.911	+1.0225	+9.5846	−50.905	−9.9058	+26.223
	2	+31.253	+1.3358	+12.298	−63.839	−12.706	+32.892
MQPM	3	+39.676	+1.7640	+15.962	−81.005	−16.485	+41.740
	4	+50.976	+2.3542	+20.955	−104.01	−21.632	+53.598
	5	+66.281	+3.1738	+27.817	−135.15	−28.700	+69.640
	6	+87.205	+4.3204	+37.325	−177.68	−38.485	+91.542
	0	+17.509	+0.7914	+7.0682	−33.572	−6.8313	+16.166
	1	+21.713	+1.0225	+8.9655	−41.627	−8.6632	+20.050
	2	+27.238	+1.3358	+11.504	−52.208	−11.113	+25.151
ISM	3	+34.576	+1.7640	+14.932	−66.252	−14.418	+31.919
	4	+44.418	+2.3542	+19.603	−85.078	−18.920	+40.990
	5	+57.748	+3.1738	+26.024	−110.56	−25.103	+53.262
	6	+75.969	+4.3204	+34.920	−145.36	−33.663	+70.018

first and higher moments. The two regions where the ellipse and the bundle cross each other correspond to positive and negative values of s, and are enlarged in the lower set of panels. As discussed in Appendix B, in principle there are two other regions of crossing, close to the extremal sides of the ellipse and thus beyond scale (not shown), that would correspond to unphysical values of r (much smaller or much larger than unity).

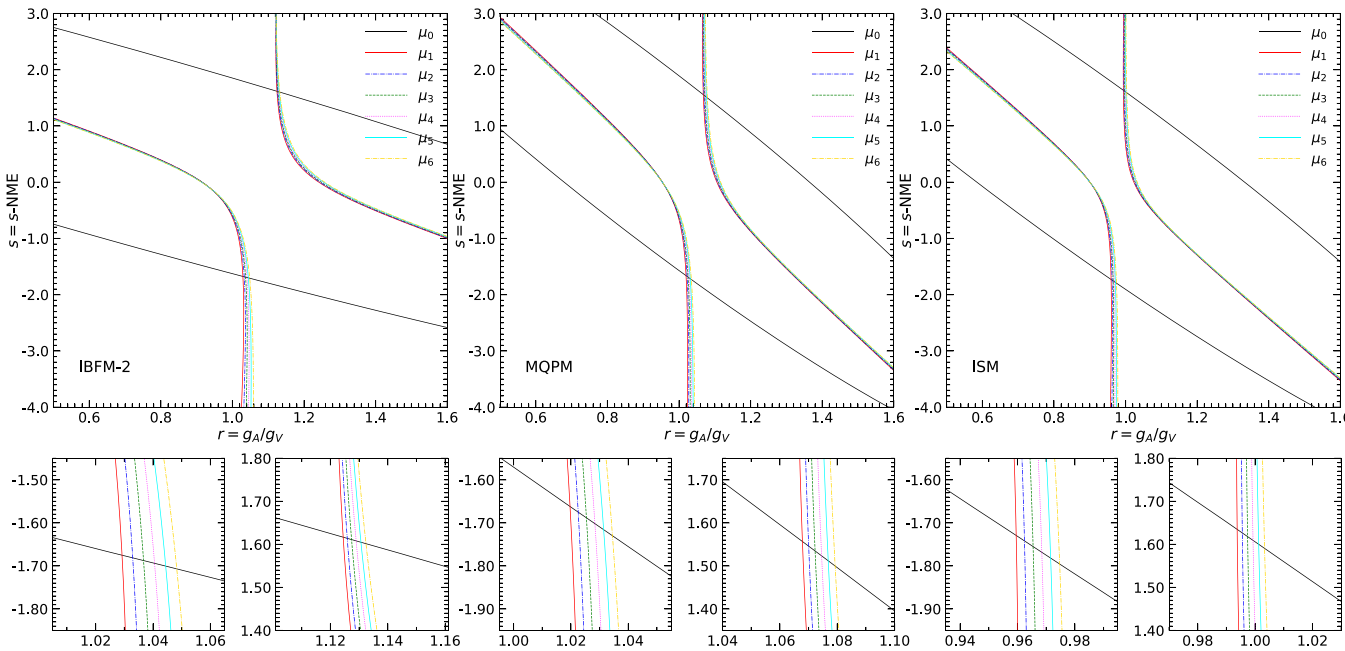

FIG. 3. Numerical results obtained by imposing the equality of theoretical and experimental moments, $\mu^t_n = \mu^e_n$ (up to $N = 6$) in the plane charted by the free parameters $r = g_A/g_V$ and $s = s$-NME. The left, middle, and right plots correspond to the IBFM-2, MQPM, and ISM models, respectively. In each of the three upper panels, note (part of) the slanted ellipse determined by the zeroth moment, and the bundle of hyperbolas determined by the first and higher moments. For each model, the two lower panels zoom in the regions at $s < 0$ (left) and $s > 0$ (right) where the ellipse and the bundle cross each other. See the text for details.

TABLE II. Intersection points of the zeroth- and first-moment curves in the (r, s) plane, for each of the three nuclear models considered.

Model	r	s
IBFM-2	1.125	+1.617
	1.029	−1.675
MQPM	1.068	+1.557
	1.020	−1.662
ISM	0.994	+1.635
	0.960	−1.729

In each of the enlarged crossing regions reported in Fig. 3 (lower panels), the bundle of hyperbolas shows some dispersion, that turns out to be smaller for $s > 0$ as compared with $s < 0$, and minimal for the IBFM-2 model. Therefore, we expect that the experimental spectrum is best matched by the theoretical spectra at $s > 0$ (with respect to $s < 0$), in particular for the IBFM-2 model. For definiteness, we check these expectations by calculating the S^t spectra at the points where the μ_0 ellipse intersects the μ_1 hyperbola, whose coordinates as reported in Table II.

Figure 4 shows the theoretical spectra corresponding to the above (r, s) values for the three nuclear models: IBFM-2 (left), MQPM (middle), and ISM (right). In each panel, the experimental spectrum (in light blue) should be compared with the blue-dashed and red-dotted spectra, referring to positive and negative values of s in Table II, respectively. The spectra with $s > 0$ are generally slightly broader and less peaked than the experimental spectrum, while the opposite happens for the spectra with $s < 0$. The deviations from the experimental spectrum are generally smaller for $s > 0$ than for $s < 0$. and can be as small as the experimental errors for the IBFM-2 model at $s > 0$. In this context, we recall that the model IBFM-2 predicts *a priori* $s = 0$ [18], and that only by fixing $s \approx 1.6$ does one get the good agreement with the experimental data in Fig. 4; see Appendix A for details.

We thus find that all models point towards $r \approx 1$, corresponding to a quenching factor $q = g_A/g_A^{\rm vac} \approx 0.8$ assuming $g_V = 1$; and towards $|s| \simeq 1.6$, corresponding to a small vectorlike relativistic NME in the expected ballpark of $O(1)$, with a preference for $s > 0$. More precisely, by grouping the values in Table II, we find the best match between theory and data around

$$r \simeq 0.99 - 1.13, \tag{29}$$

$$s \simeq 1.56 - 1.64, \tag{30}$$

with a secondary (worse) match around $r \simeq 0.96$–1.03 and $s = -(1.66$–$1.73)$, that cannot be excluded *a priori* from a phenomenological viewpoint (see also Appendix A). Remarkably, the above ranges correspond to relatively small uncertainties on the (r, s) parameters.

It would be tempting to refine the indications in favor of $r \approx 1$ and $|s| \approx 1.6$ by attaching more accurate error estimates to these parameters, as derived by detailed data fits including both experimental and theoretical uncertainties. However, in our case the theoretical shape errors are likely to be larger than the data errors (in contrast with the data analysis in [19]), as suggested by the fact that, in Fig. 4, the theoretical spectra are generally outside (or at border of) the experimental error band. As a check, we have performed numerical least-squares adjustments of the theoretical spectra by including only experimental uncertainties, either by fitting the binned spectrum with uncorrelated total errors in Fig. 1 or by fitting the associated $N = 6$ moments with their propagated covariance matrix. In both cases we obtain unreasonably high values of the minimum χ^2 per degree of freedom (d.o.f.) (except for the noted IBFM-2 case at $s > 0$), and unreasonably tiny errors on (r, s) at the subpercent level (in all cases), that are much smaller than the realistic few-percent spread of the same parameters (see Table II). On the positive side, by using only experimental errors, the (r, s) best fits are invariably close to the $s > 0$ solutions reported in Eqs. (29) and (30) and their associated spectra are close to those in Fig. 4, within percent-level deviations (not shown). The SMM appears thus to provide reasonably correct and robust (r, s) values, even with a limited amount of information and without the need for detailed data

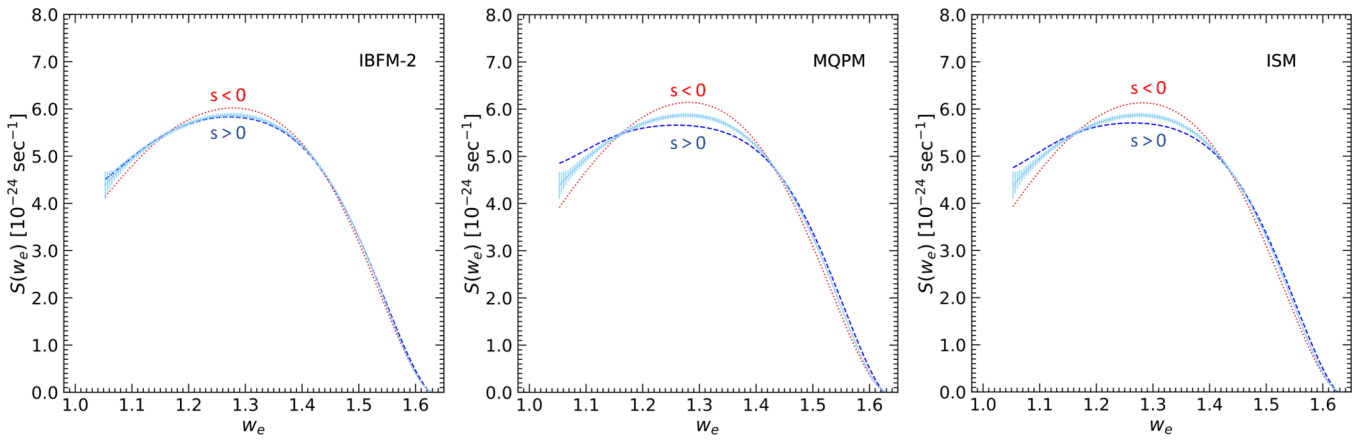

FIG. 4. Theoretical spectra calculated at the (r, s) points reported in Table II, for each of the three nuclear models IBMF-2, MQPM, and ISM (left, middle, and right panels), as compared with the experimental spectrum of Fig. 1. In each panel, the dashed blue curve refers to the case $s > 0$, and the dotted red curve to the case $s < 0$.

TABLE III. The single-particle matrix elements ${}^{V}\mathcal{M}^{(0)}_{431}$ (fm^3) for ^{113}Cd for the relevant orbitals.

	$0f_{7/2}$	$0f_{5/2}$	$1p_{3/2}$	$1p_{1/2}$	$0g_{9/2}$	$0g_{7/2}$	$1d_{5/2}$	$1d_{3/2}$	$2s_{1/2}$	$0h_{11/2}$
$0f_{7/2}$	0	0	0	0	0	0	0	0	0	9.5
$0f_{5/2}$	0	0	0	0	0	0	0	0	0	−4.3
$1p_{3/2}$	0	0	0	0	0	0	0	0	0	−12.5
$1p_{1/2}$	0	0	0	0	0	0	0	0	0	0
$0g_{9/2}$	0	0	0	0	0	0	0	0	0	0
$0g_{7/2}$	0	0	0	0	0	0	0	0	0	0
$1d_{5/2}$	0	0	0	0	0	0	0	0	0	0
$1d_{3/2}$	0	0	0	0	0	0	0	0	0	0
$2s_{1/2}$	0	0	0	0	0	0	0	0	0	0
$0h_{11/2}$	−9.5	−4.3	12.5	0	0	0	0	0	0	0

fits. Future improvements may include theoretical spectrum shape errors as estimated, e.g., by a detailed analysis of the inputs or approximations inherent the current next-to-leading order NME calculations in each nuclear model; a task that is beyond the scope of this work.

Similar results on (r, s) were obtained in [19], by applying a revised spectrum shape approach to an independent set of ^{113}Cd β-decay data, characterized by a higher threshold ($T_{\rm thr} \simeq 52$–132 keV in different detectors, with $\langle T_{\rm thr}\rangle = 92$ keV) with respect to the data used herein [16] (having a single $T_{\rm thr} = 26$ keV). In [19], the preferred values for the free parameters were found to cluster around $g_{\rm A} \simeq 0.83$–0.99 (somewhat lower than our $g_{\rm A} \approx 0.99$–1.13) and around $s \simeq 1.85$–2.1 (somewhat higher than our $s \simeq 1.56$–1.64). We surmise that these differences may be due in part to the different ^{113}Cd data sets and in part to the different approach used in the analysis. In particular, in this work the spectrum normalization is constrained through the zeroth moment (i.e., the absolute decay rate μ_0 above the 16 keV threshold), while in [19] it is constrained through the decay half-life (that requires a spectrum extrapolation below each of the 52–132 keV detector thresholds). As noted at the end of Sec. II A, such extrapolations may lead to biases. Altering the normalization leads to anticorrelated changes between $g_{\rm A}$ and s (as suggested by the μ_0 ellipse in our approach), which is what we find in comparison with [19]. Apart from these differences, a robust message emerges from [19] and from this work: Quenched values of the axial-vector coupling (around $g_{\rm A} \simeq 0.9$–1), accompanied by an adjustment of the small vector NME (around $s \simeq 1.6$–2), are required to match the existing ^{113}Cd β-decay spectrum data in both normalization and shape, in each of the three nuclear models considered.

Around these (r, s) values, large NME cancellations take place, leaving residual spectra that reasonably reproduce the experimental spectrum both in normalization (zeroth moment) and in shape (first and higher moments). These phenomenological facts strongly suggest that all the models require the following adjustments: An overall multiplicative correction to the axial-vector NME, via a quenched value $g_{\rm A} \approx 1$ (for $g_V = 1$); and a small additive vectorlike correction, parametrized by a s-NME with an absolute value around $s \approx 1.6$. One might wonder whether $g_{\rm V}$ could be used as free parameters instead of s, abandoning the CVC assumption $g_V = 1$. The answer is negative, since the prefactor $g_{\rm V}^2$ in Eq. (23) would only affect the zeroth moment μ_0 but would cancel out in the first and higher moments [Eq. (8)], leading to a spectrum shape depending on a single free parameter r. It was already concluded in [15] that one cannot match both the spectrum normalization and its shape by varying just $g_{\rm V}$ besides $g_{\rm A}$. In other words, the additive adjustment parametrized by s cannot be traded for a multiplicative adjustment parametrized by $g_{\rm V}$. At present, the CVC assumption $g_{\rm V} = 1$ can thus be safely maintained in the context of ^{113}Cd β decay.

TABLE IV. The single-particle matrix elements ${}^{V}\mathcal{M}^{(0)}_{440}$ (fm^4) for ^{113}Cd for the relevant orbitals.

	$0f_{7/2}$	$0f_{5/2}$	$1p_{3/2}$	$1p_{1/2}$	$0g_{9/2}$	$0g_{7/2}$	$1d_{5/2}$	$1d_{3/2}$	$2s_{1/2}$	$0h_{11/2}$
$0f_{7/2}$	434	319	−363	−426	0	0	0	0	0	695
$0f_{5/2}$	−319	336	484	0	0	0	0	0	0	−306
$1p_{3/2}$	−363	−484	0	0	0	0	0	0	0	−907
$1p_{1/2}$	426	0	0	0	0	0	0	0	0	0
$0g_{9/2}$	0	0	0	0	729	382	−644	−397	637	0
$0g_{7/2}$	0	0	0	0	−382	621	452	−501	−570	0
$1d_{5/2}$	0	0	0	0	−644	−452	583	820	0	0
$1d_{3/2}$	0	0	0	0	397	−501	−820	0	0	0
$2s_{1/2}$	0	0	0	0	637	570	0	0	0	0
$0h_{11/2}$	695	306	−907	0	0	0	0	0	0	1111

TABLE V. The single-particle matrix elements ${}^{A}\mathcal{M}^{(0)}_{441}$ (fm^4) for ^{113}Cd for the relevant orbitals.

	$0f_{7/2}$	$0f_{5/2}$	$1p_{3/2}$	$1p_{1/2}$	$0g_{9/2}$	$0g_{7/2}$	$1d_{5/2}$	$1d_{3/2}$	$2s_{1/2}$	$0h_{11/2}$
$0f_{7/2}$	0	500	−160	−475	0	0	0	0	0	−301
$0f_{5/2}$	500	0	−538	0	0	0	0	0	0	615
$1p_{3/2}$	160	−538	0	0	0	0	0	0	0	794
$1p_{1/2}$	−475	0	0	0	0	0	0	0	0	0
$0g_{9/2}$	0	0	0	0	0	774	−283	−624	565	0
$0g_{7/2}$	0	0	0	0	774	0	−704	222	632	0
$1d_{5/2}$	0	0	0	0	283	−704	0	911	0	0
$1d_{3/2}$	0	0	0	0	−624	−222	911	0	0	0
$2s_{1/2}$	0	0	0	0	−565	632	0	0	0	0
$0h_{11/2}$	301	615	−794	0	0	0	0	0	0	0

IV. SUMMARY AND PERSPECTIVES

In this work we have studied the normalization and shape of the electron energy spectrum of the fourth-forbidden β decay of ^{113}Cd with a novel approach, coined the spectral-moment method (SMM), based on a truncated set of spectral moments μ_n. The zeroth moment is related to the normalization, while the first and higher moments are related to the shape. As in [19], we have assumed that the spectra depend on two free parameters: An axial-vector coupling parameter $r = g_A/g_V$ (for $g_V = 1$) and a small relativistic vectorlike NME parameter s. We have shown that each moment is a quadratic form in (r, s); isomoment curves are ellipses for μ_0 and hyperbolas for $\mu_{1,2,3,...}$; and the intersections of a few moment curves are enough to derive interesting constraints on (r, s), without detailed data fits (see also Appendix B).

In particular, by equating the theoretical moments with the experimental ones, as derived from the data in [28], the following results emerge: The intersection of the μ_0 and μ_1 curves provides $r \approx 1$ and $|s| \approx 1.6$; the case $s > 0$ results in a smaller spread of intersections with higher-moment curves and is thus preferred, as also confirmed by visual inspection of the spectra. Nuclear model considerations also suggest $s \geqslant 0$, although $s < 0$ cannot be excluded *a priori* (see also Appendix A). The spread of the (r, s) values in Table II, at the level of a few percent at least, exceeds the purely experimental uncertainties and calls for (currently unquantified) theoretical spectrum-shape uncertainties. In any case, our results are in the same ballpark as those obtained in [19] with a different methodology and independent data. In general, the derived (r, s) values provide evidence for a multiplicative renormalization (quenching) of the axial coupling g_A and for an additive adjustment of vectorlike terms via the small relativistic s-NME.

Since the main quantitative information (apart from indications about the sign of s) has been derived just from μ_0 and μ_1, we surmise that the SMM can be quite powerful even when the experimental data are less accurate than those used in this work for ^{113}Cd. In this context, it should be noted that ^{113}Cd is just one of several nuclei where forbidden β decays occur with a significant spectral dependence on g_A [15,24,34,35] and possibly on other parameters such as the s-NME or similar ones.

In cases where the available spectral data are scarce, it should anyway be possible to derive, within a specified energy window $w_e \in [w_e^{\min}, w_e^{\max}]$, at least the spectrum normalization (μ_0) and the average energy (μ_1) with reasonable approximation. By equating the experimental and theoretical values for these two moments, constraints on (r, s) or equivalent parameters could be derived, without the need of complicated data fits. Among the forbidden β-decay spectra with significant g_A dependence, of particular importance is the ^{115}In spectrum [15], that was experimentally observed long ago in [36] and recently measured with a bolometric detector in [25]. A first data analysis with the spectrum-shape method (SSM), and using only g_A as a free parameter, suggests significant g_A quenching [25] but does not account for both normalization and shape at the same time. It remains to be seen if allowance for an extra parameter such as the s-NME can provide a match to all data. The presently introduced SMM might allow a rapid check of this possibility, and will be applied to, e.g., existing ^{115}In data in a separate work.

ACKNOWLEDGMENTS

The work of E.L. and A.M. is partly supported the Italian Ministero dell'Università e Ricerca (MUR) through the research Grant No. 2017W4HA7S, "NAT-NET: Neutrino and Astroparticle Theory Network" under the program PRIN 2017, and by the Istituto Nazionale di Fisica Nucleare (INFN) through the "Theoretical Astroparticle Physics" (TAsP) project. We are grateful to P. Belli, R. Bernabei, F. A. Danevich, and V. I. Tretyak for providing us with a digitized form of the ^{113}Cd β-decay spectrum data [16] as updated in Fig. 29 of [28], and for useful correspondence.

APPENDIX A: ANALYSIS OF RELEVANT NME

In the Tables III–V we have listed the single-particle (s.p.) matrix elements corresponding to all relevant transitions in the vector and axial-vector NME of interest for our analysis, namely, the small $s = {}^{V}\mathcal{M}^{(0)}_{431}$ and the large (and largely canceling) terms ${}^{V}\mathcal{M}^{(0)}_{440}$ and ${}^{A}\mathcal{M}^{(0)}_{441}$. The relevant prefactors have been included so that these correspond to single-particle model NME and are thus comparable to the numerical NME values listed in [18] for ^{113}Cd.

Given that the initial and final states are ground states with spin-parities $1/2^+$ and $9/2^+$, respectively, the transition is most likely dominated by a transition between the neutron orbital $2s_{1/2}$ and the proton orbital $0g_{9/2}$. This means ${}^V\mathcal{M}^{(0)}_{431}(\text{s.p.}) = 0$ fm^3, ${}^V\mathcal{M}^{(0)}_{440}(\text{s.p.}) = 637$ fm^4, and ${}^A\mathcal{M}^{(0)}_{441}(\text{s.p.}) = 565$ fm^4. The nuclear models give ${}^V\mathcal{M}^{(0)}_{440} =$ 317–827 fm^4, and ${}^A\mathcal{M}^{(0)}_{441} =$ 314–848 fm^4, which are in reasonable agreement with the single-particle NME with the final values depending on contributions from other nearby orbitals. For ${}^V\mathcal{M}^{(0)}_{431}$ the situation is however very different, as no orbitals near the Fermi-surface have nonzero contributions. Furthermore, the CVC relation ${}^V\mathcal{M}^{(0)}_{431} = 0.0678(R^{-1}){}^V\mathcal{M}^{(0)}_{440}$ mentioned in Sec. II D (which does not apply exactly when multiple configurations are allowed for the wave functions) suggests that ${}^V\mathcal{M}^{(0)}_{431}(\text{MQPM, CVC}) =$ 9.7 fm^3, ${}^V\mathcal{M}^{(0)}_{431}(\text{IBFM-2, CVC}) = 3.7$ fm^3, and ${}^V\mathcal{M}^{(0)}_{431}(\text{ISM}) =$ 8.4 fm^3, while the models give the values 0.37 fm^3, 0 fm^3, and 0 fm^3, respectively. For the CVC values for the smallest NME to hold, the transition would need to be basically a pure $0h_{11/2}$-$1p_{3/2}$ which does not seem reasonable based on the spin-parities, the facts that these are ground states, and the proton and neutron numbers of the nuclei.

For ISM and IBFM-2 the value of ${}^V\mathcal{M}^{(0)}_{431}$ is systematically zero, because in the ISM calculations the orbital $0h_{11/2}$ was kept empty to reduce the large computational burden, and in IBFM-2 the initial state with spin-parity $1/2^+$ cannot be formed by pairing 0^+ and 2^+ bosons with a fermion with spin-parity $11/2^-$. For MQPM the contributions between $0h_{11/2}$ and the lower proton orbitals are included, but the contributions for the higher orbitals are not very reliable as the parameter tuning can be reasonably done only for the lowest orbitals.

Based on these arguments, we surmise that the s-NME is not well described by the nuclear models while the other NME do not suffer from the same problems. Therefore, it makes sense to take the s-NME as a tuning parameter instead of the large matrix elements. Concerning the sign of s, the option $s > 0$ is theoretically regarded as being more reasonable [19], since all the above estimates—despite being largely uncertain—typically provide $s \geqslant 0$. However, one cannot exclude *a priori* that $s < 0$, also because some single-particle contributions may be negative (see Table III).

APPENDIX B: QUADRATIC FORMS IN THE (r, s) PARAMETERS AND CONIC SECTIONS

As mentioned in Sec. II D and discussed in [19], in the (r, s) region where theoretical and experimental spectra match, subtle cancellations in S^t occur among large NME, with residuals modulated by smaller terms. Despite the complexity of the full S^t expression at next-to-leading order [18], some insights can be gained by elaborating upon Eqs. (25) and (26), and by recalling that the moments are associated with quadratic forms in both r and s.

The leading NME cancellation operating in S^t, as well as in its integral μ_0^t, takes the form of a square of a large linear term

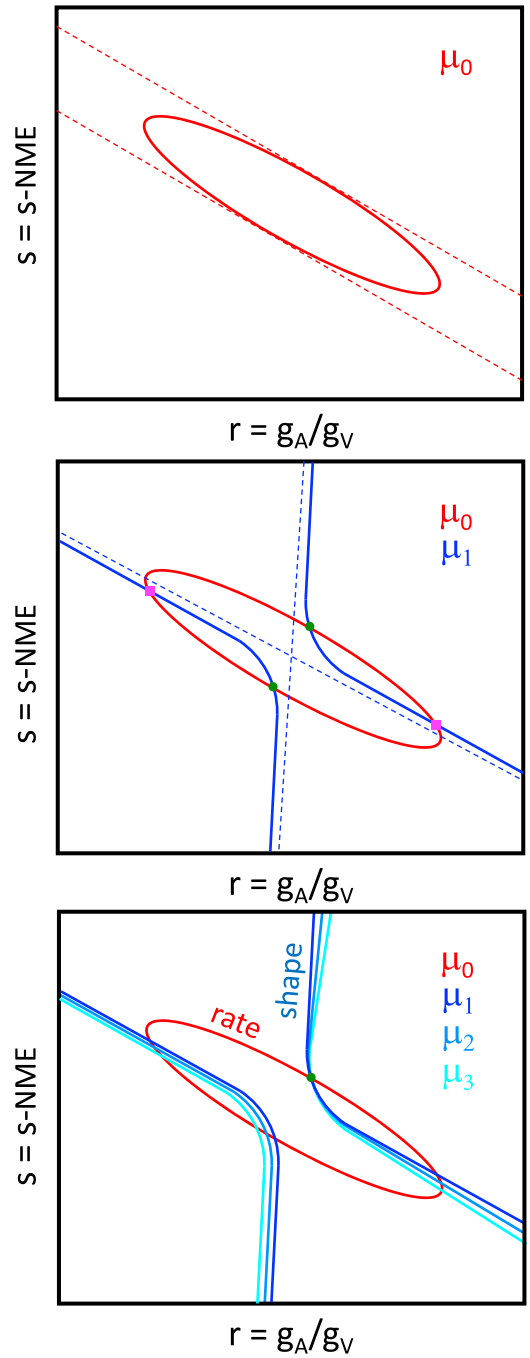

FIG. 5. Qualitative expectations for the conic sections obtained by equating the theoretical and experimental moments in the (r, s) plane (in arbitrary scales). Upper panel: Ellipse associated with μ_0, together with the degenerate limit (straight parallel lines). Middle panel: Hyperbola associated with μ_1, together with it asymptotes (roughly aligned along the vertical axis and the ellipse major axis); the hyperbola crosses the ellipse in four points (solutions). Lower panel: Bundle of hyperbolas associated with μ_1 and higher moments, crossing each other and the μ_0 ellipse at a single point (marked with a dot).

in r, modulated by a smaller term in s. In first approximation, we thus expect the zeroth moment to take the form $\mu_0^t \simeq (a - br - cs)^2 + d$, with a and b much larger than c and d. In the

plane charted by the $(r,\ s)$ parameters, the equation $\mu_0^t = \mu_0^e$ is then solved by two parallel straight lines with a small slope $-c/b$. In reality, due to subleading NME terms, the perfect square is altered into a more general quadratic form in $(r,\ s)$. Correspondingly, the two straight lines are just the degenerate limit of a conic section, which is actually an elongated and slanted ellipse.

Figure 5 (upper panel) reports graphically the above qualitative considerations in the plane charted by the r and s parameters. The elongated solid ellipse is the locus of points where $\mu_0^t = \mu_0^e$, i.e., where the normalization (event rate above threshold) of the experimental and theoretical spectra match, irrespective of their shapes that may be quite different. The dashed straight lines are a degenerate approximation of the ellipse.

While the spectrum normalization is associated with μ_0, the spectrum shape is associated with higher moments, starting from μ_1. Considering that μ_1 is a ratio of quadratic forms, the constraint $\mu_1^t(r,\ s) = \mu_1^e$ leads to a quadratic equation as well, identifying another conic section that turns out to be a hyperbola. The appearance of a hyperbola for μ_1 can be qualitatively understood as follows.

Since the denominator and numerator of μ_1 differ only by a w_e integrand of $O(1)$ in the latter [see Eq. (8)], the associated quadratic forms turn out to have nearly proportional coefficients (as confirmed by numerical inspection of Table I), corresponding to geometrically similar ellipses upon rescaling. The scaling factor turns out to be slightly more pronounced along the abscissa r, that governs the main NME cancellation term. Roughly speaking, the equation $\mu_1^t(r,\ s) = \mu_1^e$ imposes that the ratio between two very similar elliptic forms (slightly differing along the abscissa) is close to unity. If one form is written as $x^2 + y^2 - 2\rho xy$ (where x and y are generic coordinates), the other is thus obtained by scaling x as $(1+\delta)x$, where $\delta \ll 1$. It is easy to check that, at first order in δ, the ratio of these two forms is unity for either $x = 0$ (corresponding to a vertical line) or for $x = \rho y$ (a slanted line, roughly along the ellipse major axis). These two lines define a degenerate hyperbola, coincident with its two asymptotes: A vertical one and a slanted one. In general, the equation $\mu_1^t(r,\ s) = \mu_1^e$ entails a less simplistic situation: The hyperbola defined by this equation is not exactly degenerate, and its asymptotes may be slightly tilted with respect to the above expectations.

Figure 5 (middle panel) reports graphically the typical locus of points where $\mu_1^t(r,\ s) = \mu_1^e$, i.e., where the average energies of the experimental and theoretical spectra do match. The locus is a hyperbola (blue solid curve), whose branches are relatively close to the degenerate limit (asymptotes, dashed lines). The hyperbola and the ellipse will cross at four points, i.e., there will be four different (r, s) solutions to the coupled equations $\mu_0^t = \mu_0^e$ and $\mu_1^t = \mu_1^e$. In general, the extreme solutions in r (red dots) correspond to unphysically low or high values of $g_{\rm A}$, and can be discarded *a priori*; the remaining two solutions (blue dots) typically correspond to negative and positive values of s.

With a reasoning similar to μ_1, also the conic sections defined by the second or higher moments are expected to be hyperbolas. One then gets an ellipse for $n = 0$ (related to the event rate) and a bundle of hyperbolas for $n \geqslant 1$ (related to the spectrum shape). If a perfect match between theory and data can be achieved, all these conic sections must intersect in just one of the four previous points, and diverge to some extent in the others. This case is shown in the lower panel of Fig. 5, assuming the solution marked by a dot. In reality, the theory-data match is never perfect, and the intersections will be slightly separated even in the best possible case.

The above discussion allows one to understand some features of previous results reported in [19] by using the so-called revised SSM. This approach conflates the half-life and spectrum-shape methods (previously conflicting when using only r as a free parameter; see, e.g., [18]), by treating s as an additional degree of freedom. In particular, let us consider Fig. 2 of [19], showing the results of fits to an independent ^{113}Cd β-decay data set [17] in the plane charted by $g_{\rm A}$ and the s-NMA, for the same three nuclear models considered in our work. In that figure, while the half-life fit leads to an elliptical solution (akin to the ellipse determined by μ_0 in our formalism), the spectrum shape fit leads to a band that crosses the ellipse. We can interpret such a band as the path taken by the fit algorithm in [19] to follow (and to fuzzily jump across) two half-branches of the bundle of higher-moment hyperbolas, the other two halves (leading to unphysical values of $g_{\rm A}$) being discarded by construction (the fit was also restricted to $s > 0$ therein). With the spectral moment method discussed herein, the fit results in [19] can be understood in a unified picture.

[1] C. Adams, K. Alfonso, C. Andreoiu, E. Angelico, I. J. Arnquist, J. A. A. Asaadi, F. T. Avignone, S. N. Axani, A. S. Barabash, P. S. Barbeau *et al.*, Neutrinoless double beta decay, arXiv:2212.11099.

[2] M. Agostini, G. Benato, J. A. Detwiler, J. Menéndez, and F. Vissani, Toward the discovery of matter creation with neutrinoless double-beta decay, arXiv:2202.01787.

[3] V. Cirigliano, Z. Davoudi, W. Dekens, J. de Vries, J. Engel, X. Feng, J. Gehrlein, M. L. Graesser, L. Gráf, H. Hergert *et al.*, Neutrinoless double-beta decay: A roadmap for matching theory to experiment, arXiv:2203.12169.

[4] J. T. Suhonen, Value of the axial-vector coupling strength in β and $\beta\beta$ decays: A review, Front. Phys. **5**, 55 (2017).

[5] J. Suhonen and J. Kostensalo, Double β decay and the axial strength, Front. Phys. **7**, 29 (2019).

[6] J. Liu *et al.*, Determination of the Axial-Vector Weak Coupling Constant with Ultracold Neutrons, Phys. Rev. Lett. **105**, 181803 (2010).

[7] D. Mund, B. Markisch, M. Deissenroth, J. Krempel, M. Schumann, H. Abele, A. Petoukhov, and T. Soldner, Determination of the Weak Axial Vector Coupling $\lambda = g_{\rm A}/g_{\rm V}$ from a Measurement of the β-Asymmetry Parameter A

in Neutron Beta Decay, Phys. Rev. Lett. **110**, 172502 (2013).
[8] W. T. Chou, E. K. Warburton, and B. A. Brown, Gamow-Teller beta-decay rates for $A \leqslant 18$ nuclei, Phys. Rev. C **47**, 163 (1993).
[9] A. Faessler, G. L. Fogli, E. Lisi, V. Rodin, A. M. Rotunno, and F. Simkovic, Overconstrained estimates of neutrinoless double beta decay within the QRPA, J. Phys. G: Nucl. Part. Phys. **35**, 075104 (2008).
[10] J. Barea, J. Kotila, and F. Iachello, Nuclear matrix elements for double-β decay, Phys. Rev. C **87**, 014315 (2013).
[11] H. Ejiri, Nuclear matrix elements for β and $\beta\beta$ Decays and quenching of the weak coupling $g_{\rm A}$ in QRPA, Front. Phys. **7**, 30 (2019).
[12] H. Ejiri, J. Suhonen, and K. Zuber, Neutrino–nuclear responses for astro-neutrinos, single beta decays and double beta decays, Phys. Rep. **797**, 1 (2019).
[13] P. Gysbers, G. Hagen, J. D. Holt, G. R. Jansen, T. D. Morris, P. Navrátil, T. Papenbrock, S. Quaglioni, A. Schwenk, S. R. Stroberg *et al.*, Discrepancy between experimental and theoretical β-decay rates resolved from first principles, Nat. Phys. **15**, 428 (2019).
[14] V. Cirigliano, Z. Davoudi, J. Engel, R. J. Furnstahl, G. Hagen, U. Heinz, H. Hergert, M. Horoi, C. W. Johnson, A. Lovato *et al.*, Towards precise and accurate calculations of neutrinoless double-beta decay, J. Phys. G: Nucl. Part. Phys. **49**, 120502 (2022).
[15] M. Haaranen, P. C. Srivastava, and J. Suhonen, Forbidden nonunique β decays and effective values of weak coupling constants, Phys. Rev. C **93**, 034308 (2016).
[16] P. Belli, R. Bernabei, N. Bukilic, F. Cappella, R. Cerulli, C. J. Dai, F. A. Danevich, J. R. deLaeter, A. Incicchitti, V. V. Kobychev, S.S. Nagorny, S. Nisi, F. Nozzoli, D. V. Poda, D. Prosperi, V. I. Tretyak, and S. S. Yurchenko, Investigation of β decay of ^{113}Cd, Phys. Rev. C **76**, 064603 (2007).
[17] L. Bodenstein-Dresler *et al.* (COBRA Collaboration) , Quenching of $g_{\rm A}$ deduced from the β-spectrum shape of ^{113}Cd measured with the COBRA experiment, Phys. Lett. B **800**, 135092 (2020).
[18] M. Haaranen, J. Kotila, and J. Suhonen, Spectrum-shape method and the next-to-leading-order terms of the β-decay shape factor, Phys. Rev. C **95**, 024327 (2017).
[19] J. Kostensalo, J. Suhonen, J. Volkmer, S. Zatschler, and K. Zuber, Confirmation of $g_{\rm A}$ quenching using the revised spectrum-shape method for the analysis of the ^{113}Cd β-decay as measured with the COBRA demonstrator, Phys. Lett. B **822**, 136652 (2021).
[20] H. Behrens and W. Bühring, *Electron Radial Wave Functions and Nuclear Beta-decay* (Clarendon, Oxford, 1982).
[21] O. S. Kirsebom, S. Jones, D. F. Strömberg, G. Martínez-Pinedo, K. Langanke, F. K. Röpke, B. A. Brown, T. Eronen, H. O. U. Fynbo, M. Hukkanen *et al.*, Discovery of an Exceptionally Strong β-Decay Transition of ^{20}F and Implications for the Fate of Intermediate-Mass Stars, Phys. Rev. Lett. **123**, 262701 (2019).
[22] A. Kumar, P. C. Srivastava, J. Kostensalo, and J. Suhonen, Second-forbidden nonunique β-decays of ^{24}Na and ^{36}Cl assessed by the nuclear shell model, Phys. Rev. C **101**, 064304 (2020).
[23] J. V. Dawson, C. Reeve, J. R. Wilson, K. Zuber, M. Junker, C. Gossling, T. Kottig, D. Munstermann, S. Rajek, and O. Schulz, An investigation into the ^{113}Cd beta decay spectrum using a CdZnTe array, Nucl. Phys. A **818**, 264 (2009).
[24] J. Kostensalo, M. Haaranen, and J. Suhonen, Electron spectra in forbidden β decays and the quenching of the weak axial-vector coupling constant $g_{\rm A}$, Phys. Rev. C **95**, 044313 (2017).
[25] A. F. Leder, D. Mayer, J. L. Ouellet, F. A. Danevich, L. Dumoulin, A. Giuliani, J. Kostensalo, J. Kotila, P. de Marcillac, C. Nones *et al.*, Determining $g_{\rm A}/g_{\rm V}$ with High-Resolution Spectral Measurements Using a $LiInSe_2$ Bolometer, Phys. Rev. Lett. **129**, 232502 (2022).
[26] W. Feller, *An Introduction to Probability Theory and Its Applications*, 2nd ed. (Wiley, New York, 1991), Vol. II.
[27] J. A. Shohat and J. D. Tamarkin, *The Problem of Moments*, Mathematical Surveys and Monographs (AMS, Providence, 1970), Vol. I.
[28] P. Belli, R. Bernabei, F. A. Danevich, A. Incicchitti, and V. I. Tretyak, Experimental searches for rare alpha and beta decays, Eur. Phys. J. A **55**, 140 (2019).
[29] K. Schmüdgen, *The Moment Problem*, Graduate Texts in Mathematics (Springer, Berlin, 2017).
[30] N. I. Akhiezer, *The Classical Moment Problem: And Some Related Questions in Analysis* (Dover, Mineola, NY, 2020).
[31] G. Talenti, Recovering a function from a finite number of moments, Inverse Probl. **3**, 501 (1987).
[32] R. Askey, I. J. Schoenberg, and A. Sharma, Hausdorff's moment problem and expansions in Legendre polynomials, J. Math. Anal. Appl. **86**, 237 (1982).
[33] M. Wang, G. Audi, F. G. Kondev, W. J. Huang, S. Naimi, and X. Xu, The AME2016 atomic mass evaluation, Chin. Phys. C **41**, 030003 (2017).
[34] J. Kostensalo and J. Suhonen, $g_{\rm A}$-driven shapes of electron spectra of forbidden β decays in the nuclear shell model, Phys. Rev. C **96**, 024317 (2017).
[35] A. Kumar, P. C. Srivastava, and J. Suhonen, Second-forbidden nonunique β^- decays of ^{59,60}Fe: Possible candidates for $g_{\rm A}$ sensitive electron spectral-shape measurements, Eur. Phys. J. A **57**, 225 (2021).
[36] G. B. Beard and W. H. Kelly, Beta decay of naturally radioactive In-115, Phys. Rev. **122**, 1576 (1961).